Preliminary Study of the Feasibility of Coincidence Detector Using a Suspension of Superheated Superconducting Grains (SSG) in High Density Dielectric Matrix (HDDM) as Detector: examples, the Positron Emission Tomography, and Other

Roger Bruère Dawson [a,b], Jacques Maillard [b,c,g],
Gérard Maurel [d,g], Joseph Parisi [f,g] Jorge Silva [e,g],
Georges Waysand [a]

[a] *GPS UMR 7588, Universities Paris VI and Paris VII, 4 place Jussieu, 75005 Paris France*

[b] *IN2P3, 3 rue Michel Ange, 75794 Paris Cedex 16*

[c] *CNRS IDRIS, Bt 506, BP167 91403 Orsay Cedex France*

[d] *Université Paris VI, Faculté de Médecine Saint Antoine, 27 rue de Chaligny 75012 Paris France*

[e] *Université Paris VI, 4 place Jussieu, 75005, Paris, France*

[f] *Université Orsay*

[g] *MAPS, Universit Paris VI, 4 place Jussieu 75005 Paris*

Key words: Nuclear Medicine; Monte-Carlo Simulation; Micro PET; Detector; Superconductivity.

Email address: `maillard@idris.fr` (Jacques Maillard).

Presentation to Siena 2004 Topical Seminar *21 May 2004*

1 Basic Physics of SSG-HDDM

1.1 Basic physics

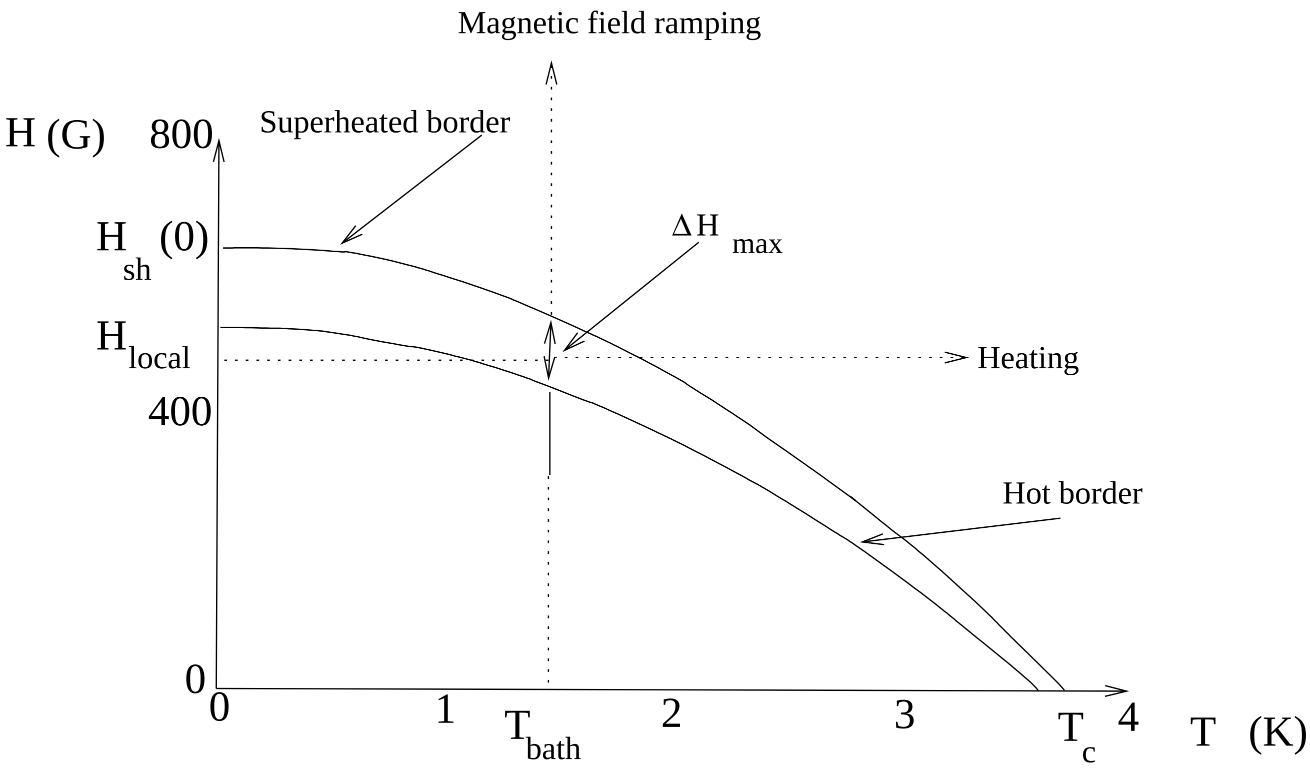

Fig. 1. Phase diagram

The delay between the moment where the particle depose the energy, and the moment where electrical signal arrives on the amplifier chain, is given by three phenomena:

- Rupture of cooper pair, the grain become norma conducting, very short (fraction of ns)
- Creation and amortissemnet of foucault current, delay of about one microsecond
- "flipping of the grain", where the field penetrates instantly and globaly in the grain (fraction of ns)

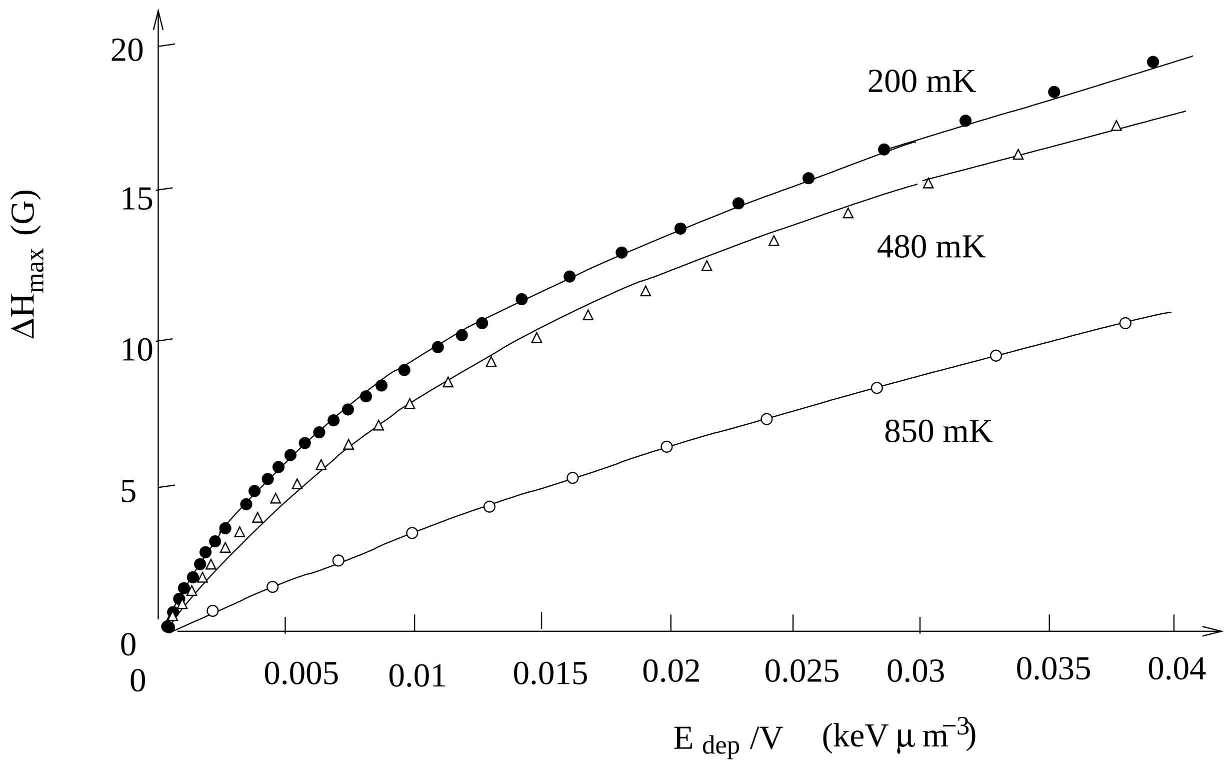

Fig. 2. Energy deposition in the grains versus ΔH_{max}. Incidently for each T_{bath} this gives the correspondence between ΔH in gauss and "ΔH " in eV.

2 Geometry of the elementary pixel of a concidence detector with HDDM-SSG

The work on SSG detector has begun in 1986. As a starting point to evaluate which kind of benefit one could expect from such a system, we take the most conservative parameters for the elementary cell:

Geometry: a cylinder 0.78 cm long ; 0.4 cm in diameter
Temperature: about 200mK
Magnetic Field: Hc (0,2K)= 300 Gauss, Hsh (0,2K)= 600 Gauss.
filling factor of 0.1 for
tin microspheres of respectively 7, 8 or 10μm radius

2.1 Experimental layout, Pratical realisation

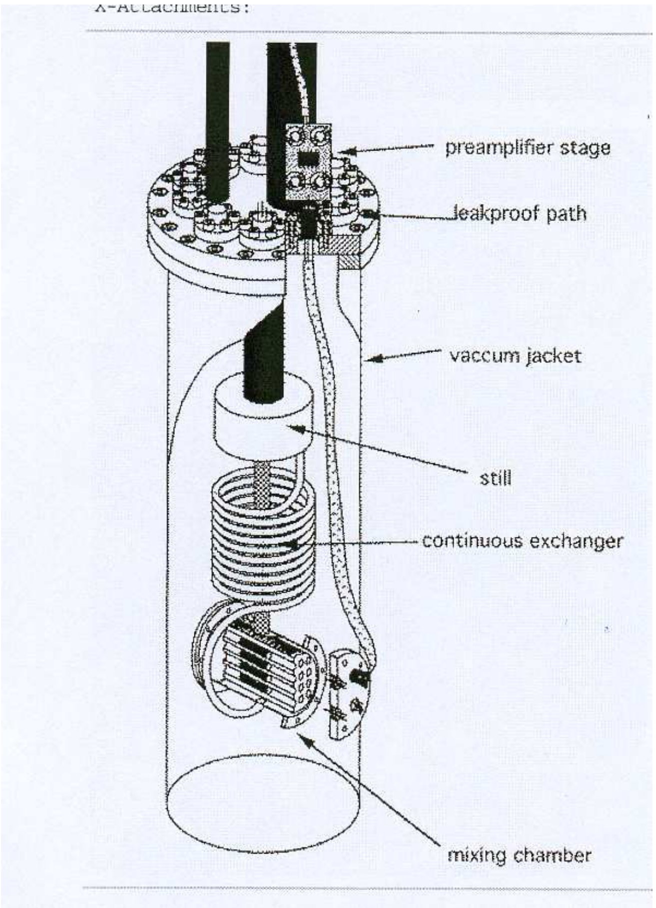

Fig. 3. Experimental design

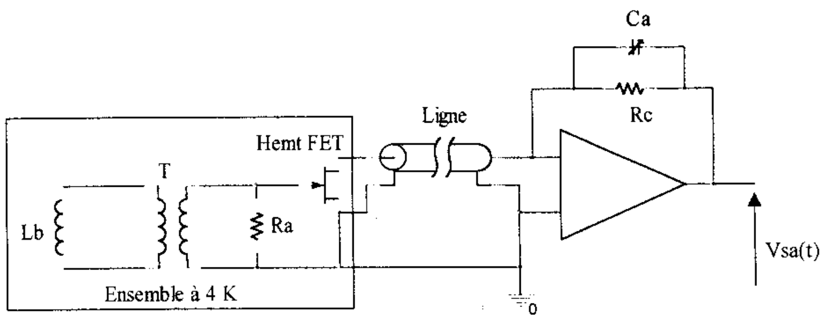

Fig 2

Le circuit de détection peut être représenté par le schéma équivalent suivant :

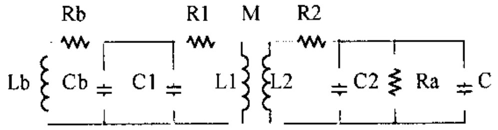

Lb : Inductance du solénoïde.
Rb : Résistance du solénoïde.
Cb : Capacité parasite du solénoïde.
C1 : Capacité parasite de l'enroulement primaire.
R1 : Résistance de l'enroulement primaire.
L1 : Inductance de l'enroulement primaire
M : Coefficient d'induction mutuelle.
L2 : Inductance de l'enroulement secondaire.
R2 : Résistance de l'enroulement secondaire.
C2 : Capacité parasite de l'enroulement secondaire.
Ra : Résistance de charge du transformateur et d'amortissement du circuit.
C : Capacité parasite de l'étage d'entrée.

Fig. 4. On line electronique

With this electronic ([1]we can amplifly 20000 time a signal, with band of 3 Mhz, which gives a 60 Ghz of quality factor. With zero crossing signal treatment algorithm, time precision can be achieved of about a few ns.

If we intend to do smaller detector, in a first order, signal amplitude is proportional to inverse of radius, the time to get the maximum apmlitude is reduced by factor 2, all caracteristic which allows, if technology of wire and grains fabrication allows it, to imagine very performant detector.

3 Deposited energies in the suspension

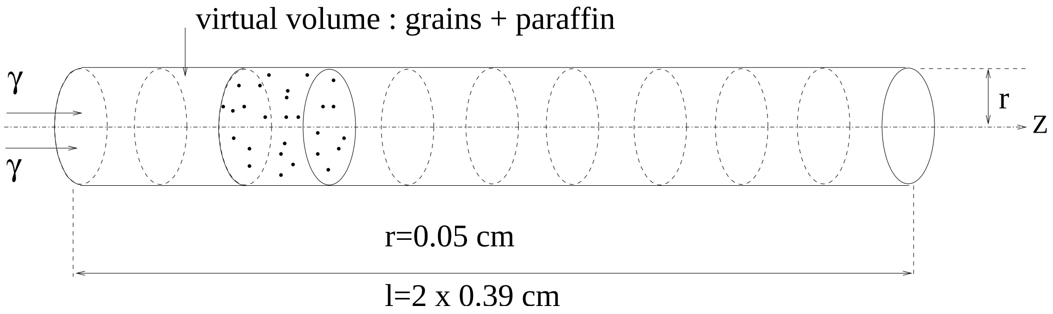

Fig. 5. Geometry of simulation

The gamma beam is parallel to the cylinder axis, arbitrarily chosen as the Z axis (5). 10^5 photons are sent onto the detector which is a suspension of mono-sized tin microspheres of either 7, 8, or 10 μm radius, representing 10% of the volume cylinder. The microspheres are immersed in a high density matrix made of litharge (Pb0, density =9.35). Such a detector irradiated by 511 keV gammas has a stopping power of about 37%: Simulation gives that out of 100 000 photons impinging on the cylinder, 36713 interact by electron production either by Compton or by photoelectric effect. As we will see the energy deposition in both processes occurs in the vicinity of the spot of materialisation of the impinging photon.

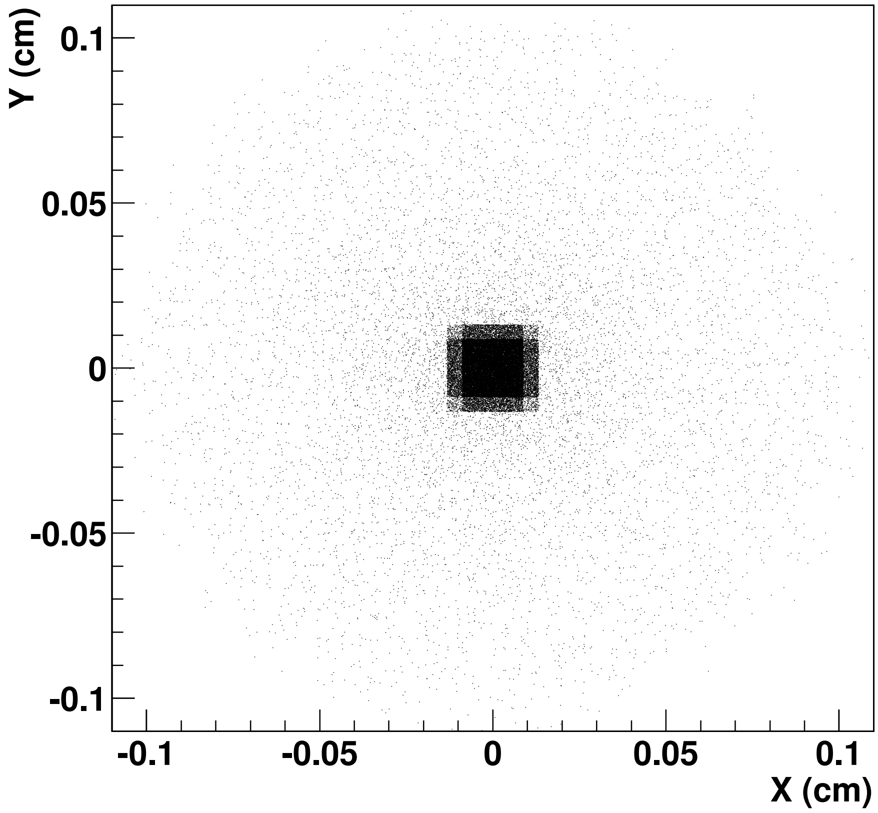

Fig. 6. xy projection of γ impact: its dispersion is one order of magnitude smaller than the radius of the simulated cylinder

Figure 6 represents the projections (X and Y) on a diametrical plane of the interaction spot of each interacting gamma in the whole cylinder. The aperture of the gamma beam is reduced to 10μm around the Z axis. In this representation one does not care if the interaction takes place in a microsphere or in the matrix. One can see that the diameter of the virtual volume is large enough to include all the diffused events.

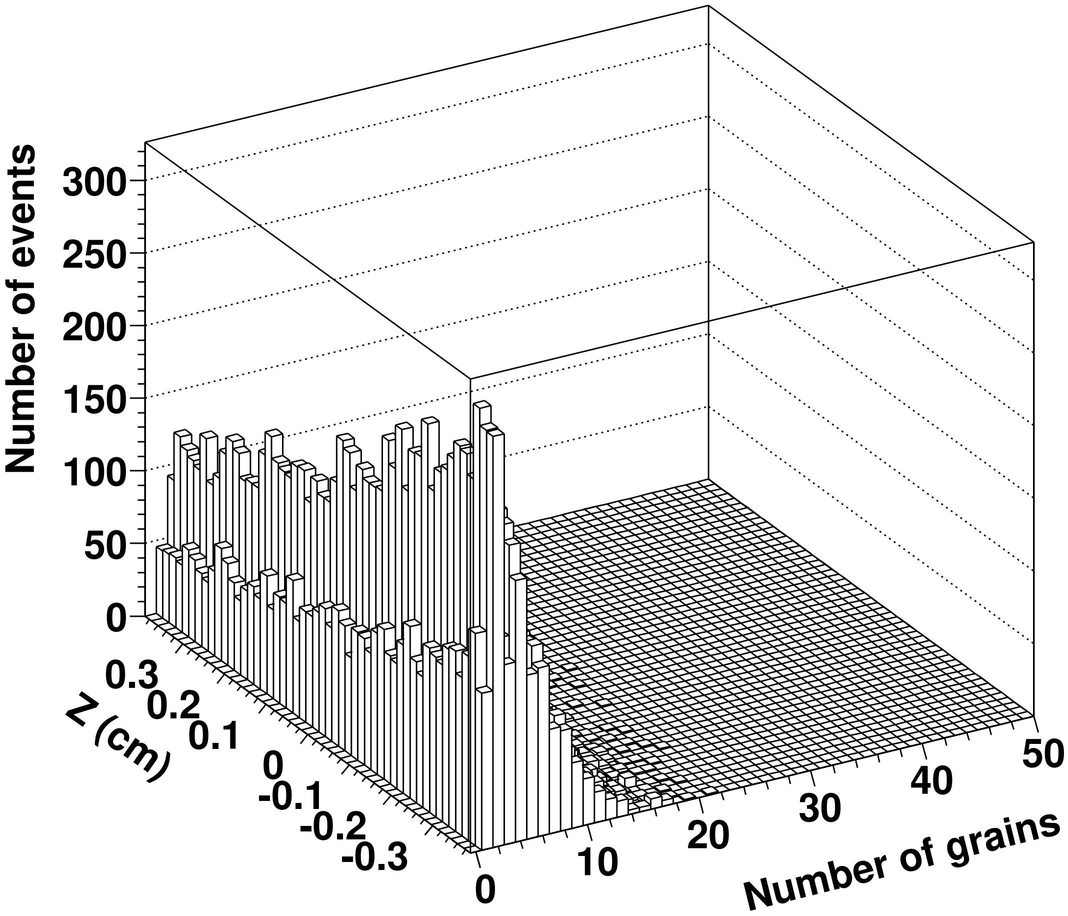

Fig. 7. Number of crossed grains versus the depth Z: the number of grains does not depend of Z

As long as the photon does not interact with the pixel there is no energy deposition. This deposition takes place only along the secondary trajectories. The energy loss useful for read-out of a photon impact occurs only in the grains. We reserve the denomination "crossed grains" or " crossed microspheres" to these specific microspheres in which there is an energy deposition. Figure 7 represents the number of crossed grains per incoming photon as a function of the depth Z in the cylinder. As expected, since the mean free path of electrons is shorter than the mean free path for photons one can see that the number of crossed granules is depth independent of the photon impact. As a result, the energy loss after a photon interaction is independent of the point where it has occurred.

3.3 Distribution of crossed grains with energy of gamma:

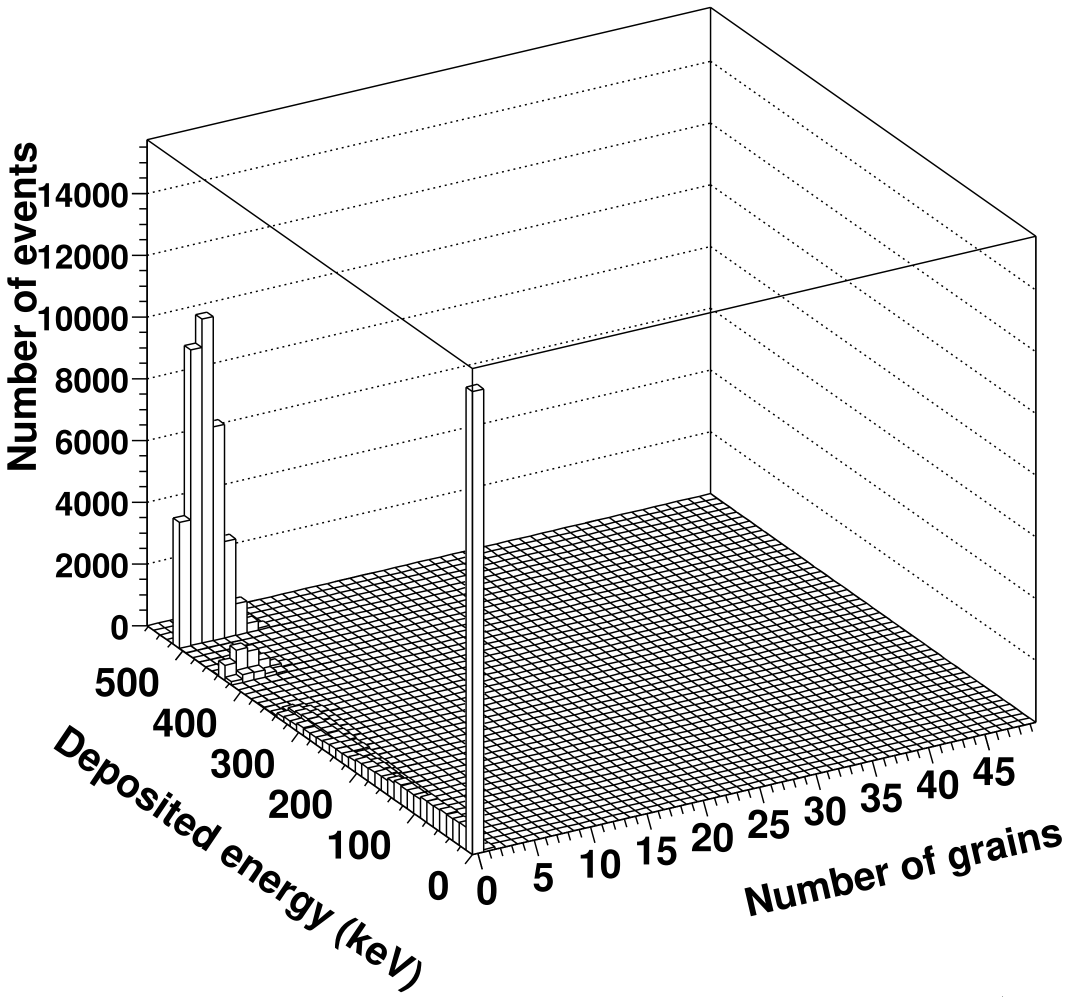

Fig. 8. Number of grains hit versus the whole energy deposition in the cell (in the litharge and in the grains)

This distribution is represented in figure 8 which gives the fraction of concerned grains for a given range of deposited energy by an impinging electron. At this stage we have a full description of the deposited energies in the suspension. So far we have not used the superconducting state properties. Now we have to estimate the response of the superheated superconducting system to this distribution of deposited energy.

3.4 Response of superheated superconducting microspheres to an energy deposition

For the purpose of the feasibility study it is enough to limit ourselves to a small number of crossed grains thus representing a tiny fraction of their overall number. In principle, for each change of state of a grain, because of the long range diamagnetic interaction, the whole set of maxima of the equatorial magnetic field is changed. However, when only a small number of grains are undergoing a transition one can assume that the distribution of maxima of the equatorial magnetic field remains the same.

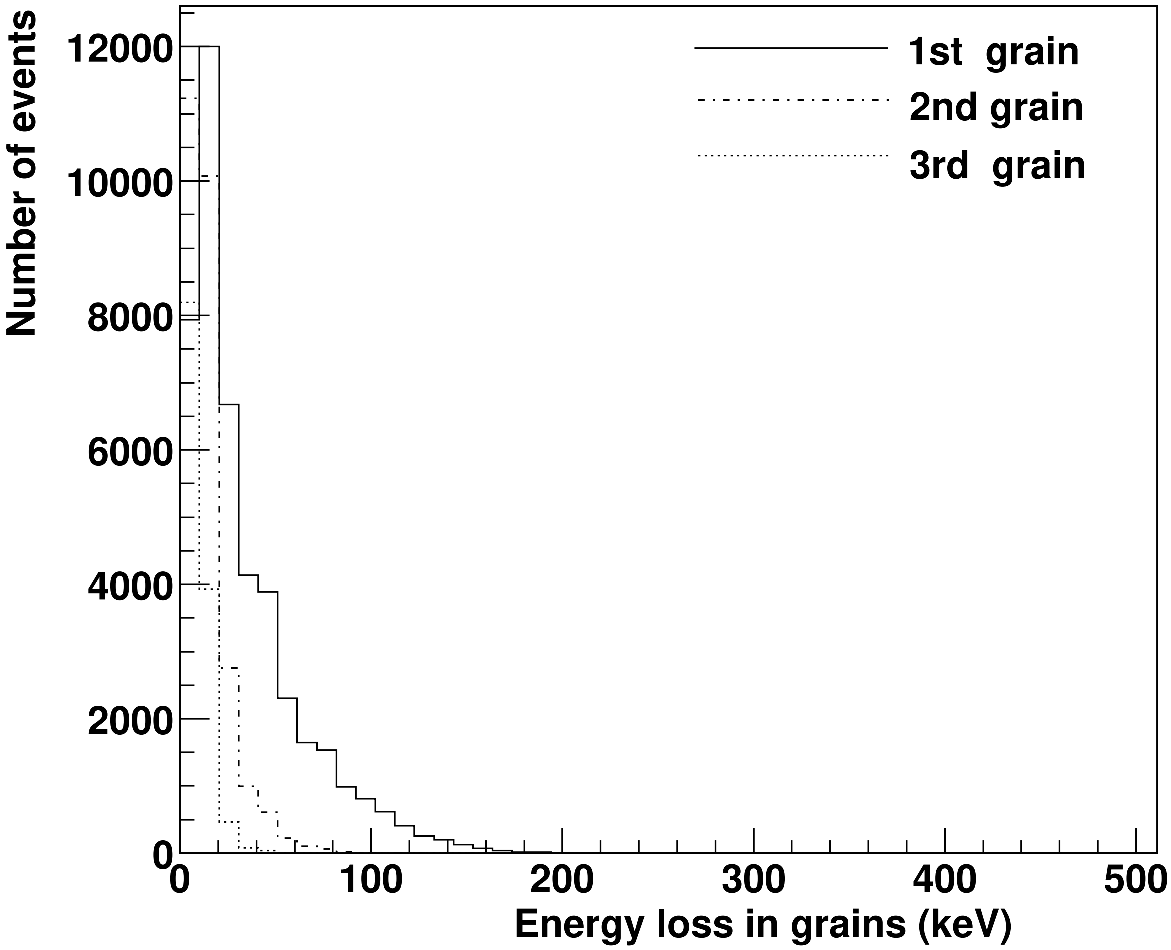

Fig. 9. Energy loss in the grains: the grains are ordered by the amount of deposited energy, the first one is represented by the continuous line

As a result the simulation relies on two quantities which, in first approximation are taken as independent stochastic phenomena:

- the energy of the gamma when entering into the grain.
- the equatorial magnetic field on the corresponding grain.

(the impact point is not a relevant parameter because the energy deposition if large enough always creates an homogeneous nucleation: there is a uniform and global heating of each flipped grain (flipped = crossed grains that will change state)). In other terms the distribution of deposited energies among crossed grains is convoluted with the distribution of their equatorial magnetic field.

Figure 2 ([2], page 82) shows the ΔH_{max} in function of the density of energy deposition in the grain, for three different temperatures. If we multiply this density by the volume of the microsphere (the grain) we get for a given temperature, and a certain energy deposition, the range of ΔH, that we can randomly choose between 0 and ΔH_{max}.

Thus we obtain as a function of the impinging photon energy the intrinsic efficiency of the pixel (figures 10,11 and 12) assuming that at H applied 20% of the grains are already flipped to the normal state and that in the interval $[H_{applied}, H_{applied}+\Delta H_{max}]$ the number of grains per unit of ΔH is constant.

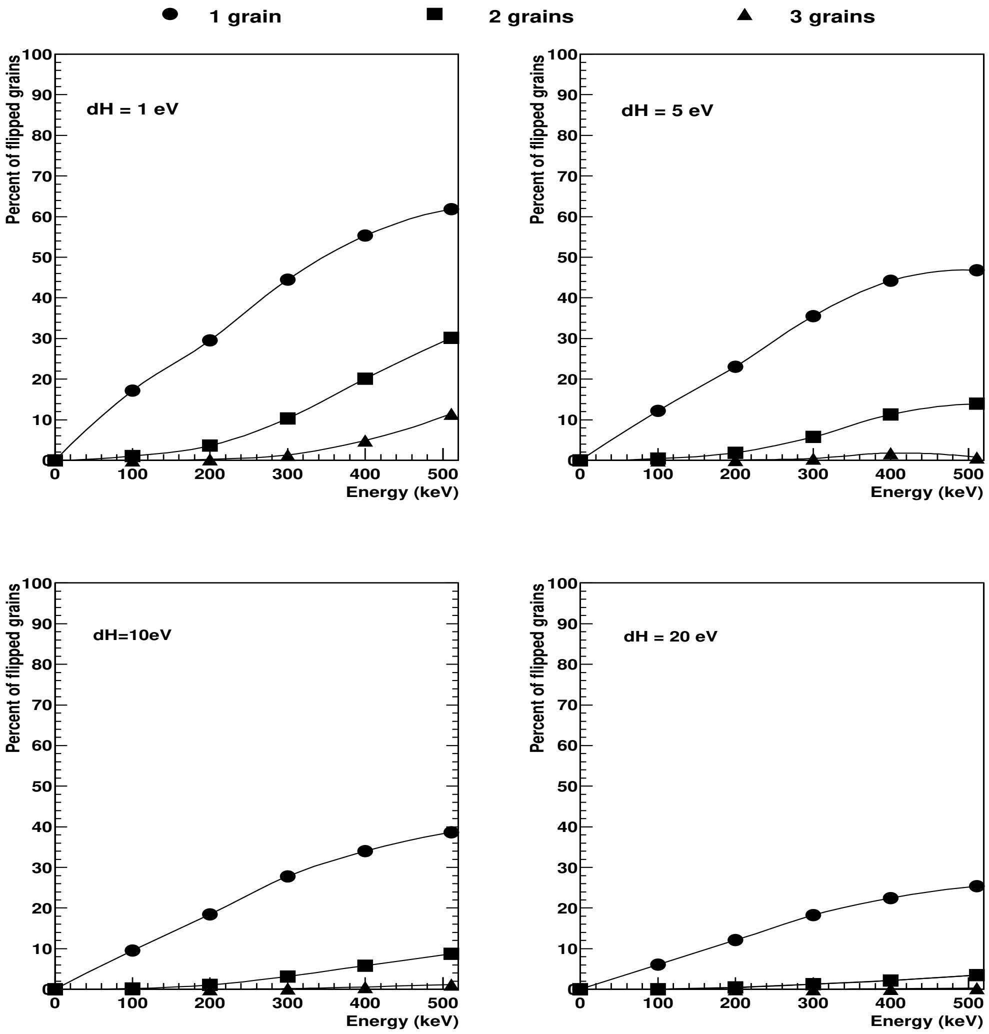

Fig. 10. Photon electronic detection efficiency in function of energy, for grains with 10 micron of radius

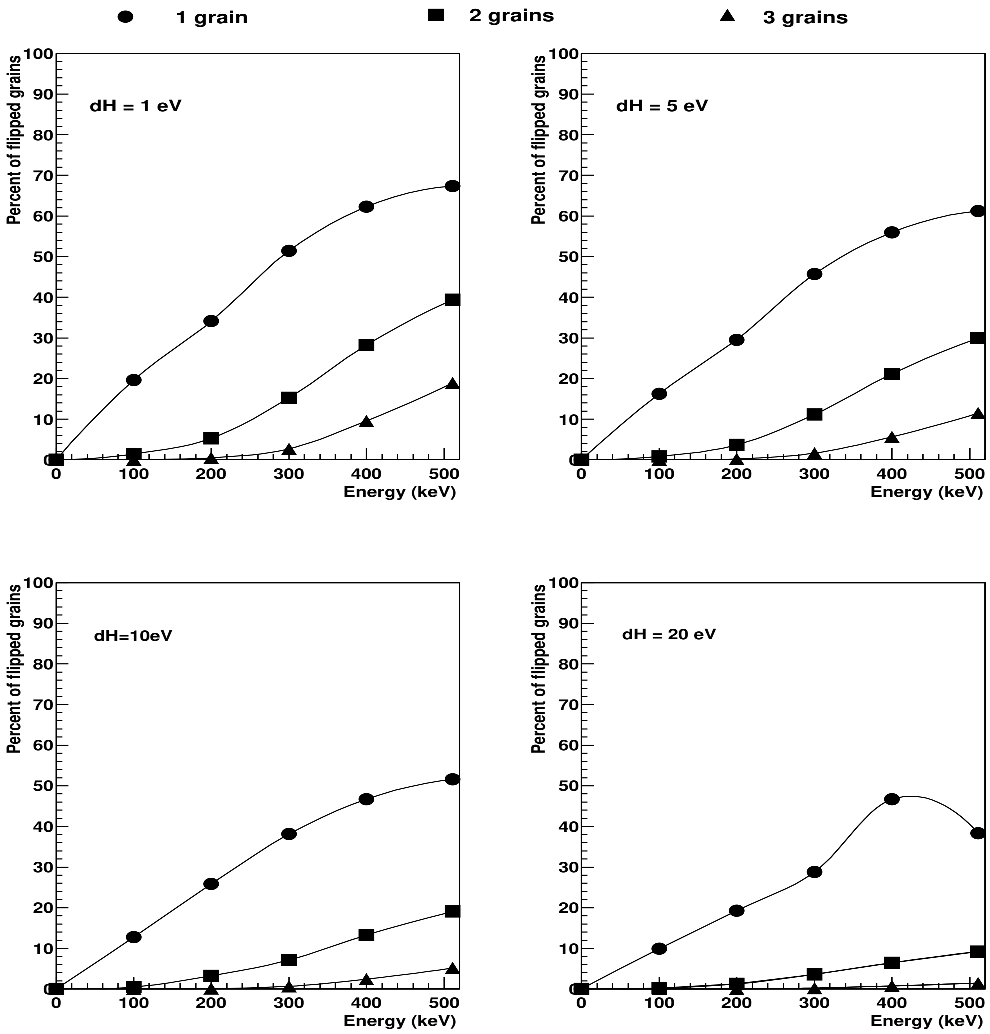

Fig. 11. Photon electronic detection efficiency in function of energy, for grains with 8 micron of radius

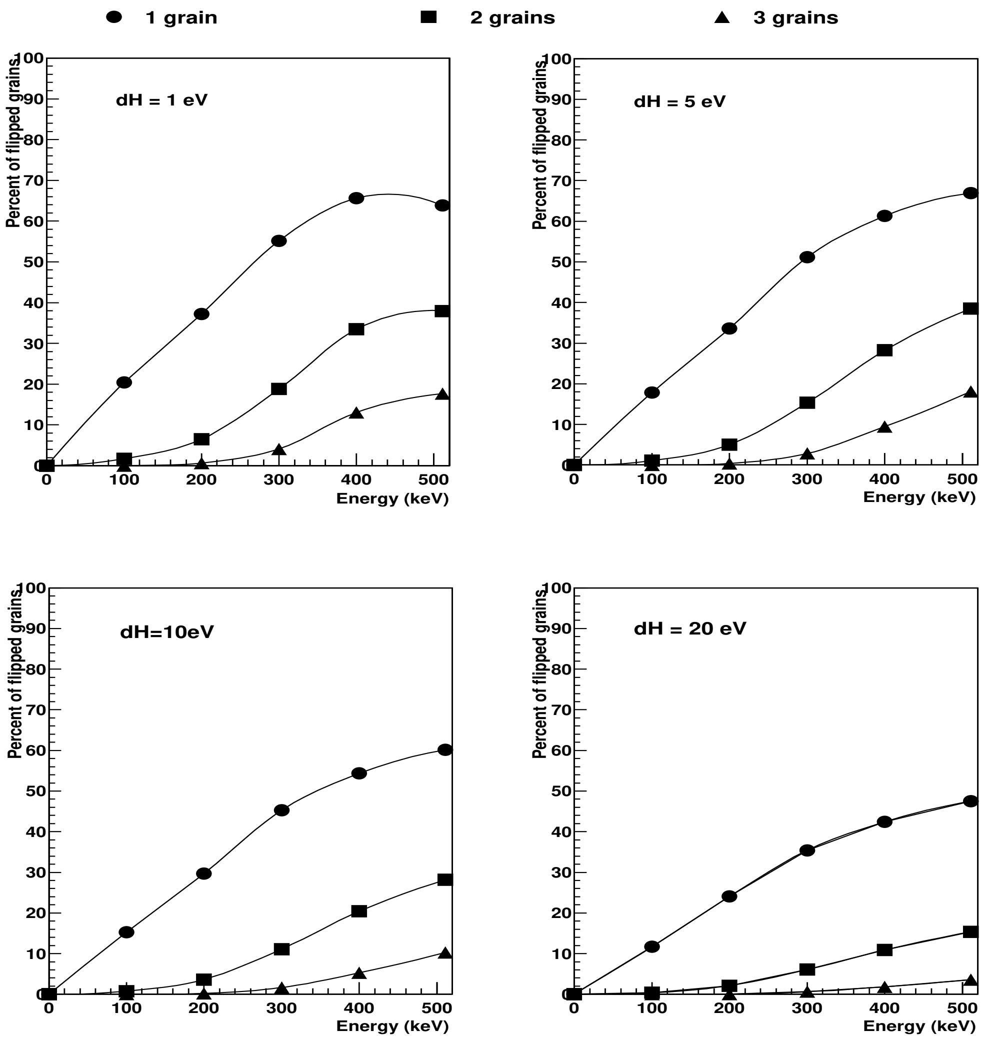

Fig. 12. Photon electronic detection efficiency in function of energy, for grains with 7 micron of radius

In fact, on figures 10, 11 and 12 for a given suspension three efficiencies have been drawn as a function of the impinging gamma respectively corresponding to the simultaneous flipping of 1, 2 or 3 grains. 3 different radius of grains has been used, 10μm, 8μm, 7μm. Four different ΔH were used, 1 eV, 5 eV, 10 eV, and 20 eV per μm^3. As expected the resulting curves are strikingly different and lead us to consider that the event selection can be based not only on energy selection by magnetic field monitoring which is conventional in SSG systems but, in that case can be combined with signal amplitude selection. This opens a wide range of configuration for PET. To appreciate the potentialities of a SSG PET let us consider the classical case of a small animal camera. The present state of art of the electronic read-out allows us to read 1 grain of 10 μm radius or 2 grains of 8 μm radius. 5 eV of ΔH is assumed. ΔH_{max} of 5 eV per cubic micron is a good compromise, allowing to work with reasonable temperature (between 200 and 500 mK, see figure 2) and precision (5 keV per μm^3) correspond to an energy loss of 20 keV in grain of 10 μm radius, see figure 9). We can for example estimate the electronic efficiency of the system at 511 keV:

- for 10 μm: 0.534
- for 8 μm: 0.380

A more sophisticated simulation shall mix the different radii of grains, allowing more subtle energy differentiation.

4 Performance required for a small animal PET

4.1 Description of the system

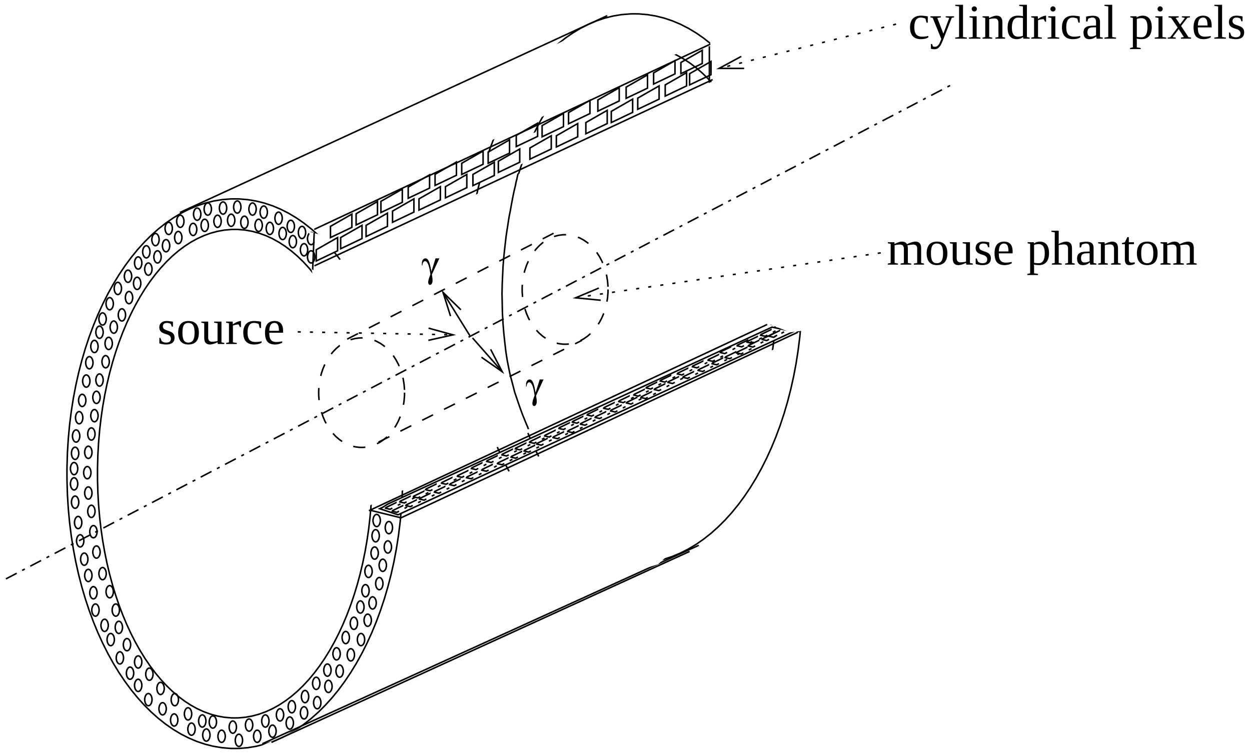

Fig. 13. Micro PET geometry

The PET requirements were discussed among others by Huber et al ([3]). One considers a mouse phantom of 29g placed in the centre of a 20 cm long cylinder, 5 cm in diameter made of two closed compact layers of elementary cylindrical pixels as discussed above (see figure 13).

Monte Carlo simulation gives a materialization efficiency (Table 1) to 511 Kev irradiation of the order of 42% in a pixel. This efficiency can be higher if one increases the depth of the detecting layer. This is possible because, contrary to classical techniques neither the read-out electronics nor the detecting material are limiting factors for an efficient design of the whole system.

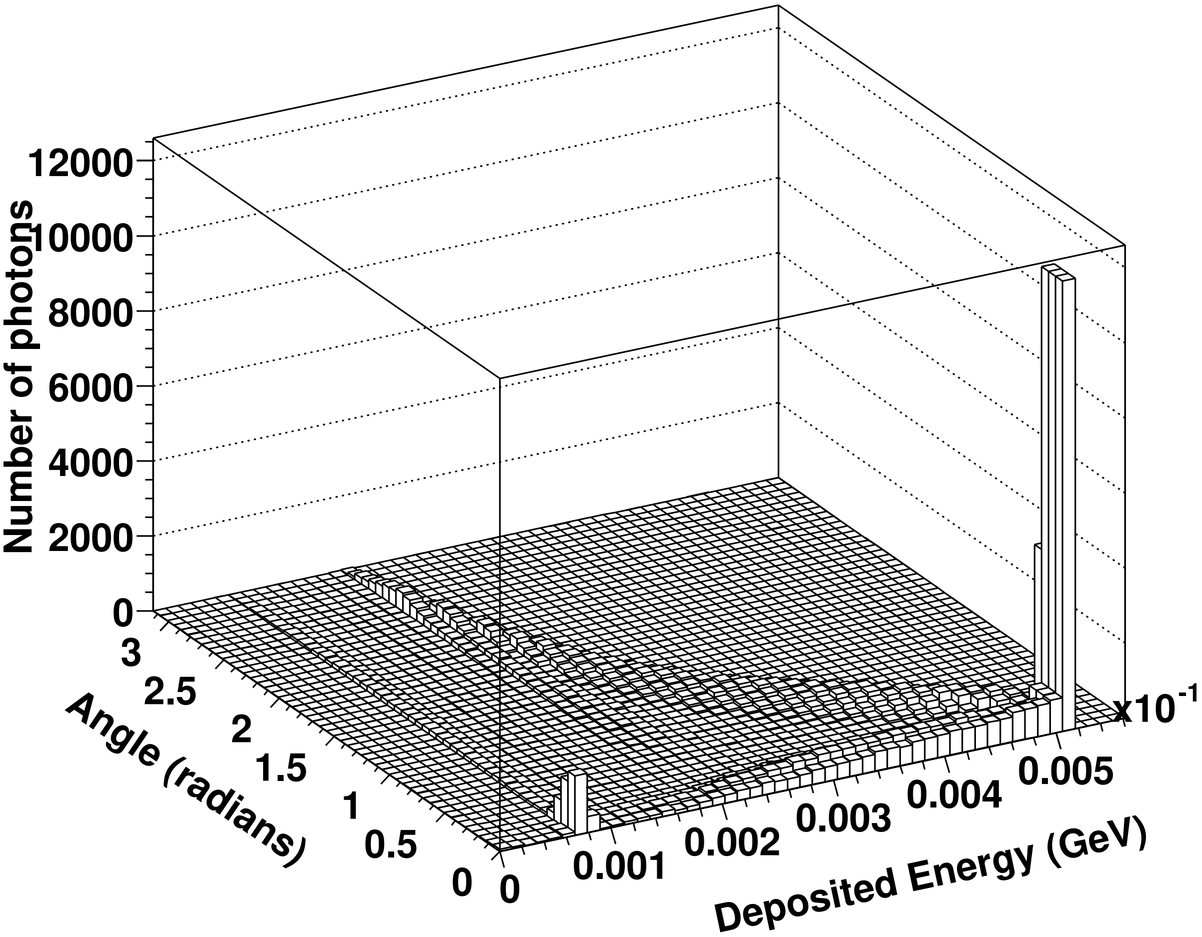

Fig. 14. Deposited energy in the cell for straight and diffused photons, versus the angle between the emitted photon and the hitted cell

The energy deposited in the pixel comes from either a straight gamma (signal) or from a diffused trajectory in the mouse phantom (noise). Figure 14 gives the distribution of the deposited energy for the straights and the diffused photons. The efficiency given by fig 7 allows an estimation of the noise equivalent counting rate (NECR) which is the ratio of interest for PET performances. For its estimation we follow conventional notations.

The true ($True$) coincidental and scatter ($Scatter$) rates are given by, μ being a constant,

$$True = \mu \cdot \rho \cdot (\epsilon^2) \cdot g_t \cdot (P^2)$$

and

$$Scatter = f_s \cdot True$$

respectively, where

ρ is the activity density,
ϵ is the single detection efficiency,
g_t is a geometry efficiency for true coincidence events,
P is the probability for escape for a 511 keV photon from the small animal,
f_s is the scatter fraction.

The random ($Random$) coincidence event rate is proportional to single event rate ($Single$)

$$2 \cdot \tau \cdot (Single)^2$$

where

$$Single = \rho \cdot \epsilon \cdot g_r \cdot P$$

that means:

$$Random = \mu \cdot 2 \cdot \tau \cdot \rho^2 \cdot \epsilon^2 \cdot g_r^2 \cdot P^2$$

and

$$Random = True \cdot \rho \cdot g_t \cdot 2 \cdot \tau$$

where

τ is the coincidence resolving time (usually 10 or 5 ns)
g_r is the geometry efficiency for random events, considered the same as g_t^2.

The Noise Equivalent Count Rate (NECR) is the number of counts detected as a function of the activity concentration, after correcting the effects of random and scatter events taking into account dead-time losses. It is a standard measure of signal to noise in reconstructed PET images.

$$NECR = True^2/(True + Scatter + k.Random)$$

where

k is a correction factor for random coincidences (k=1 or 2).

radius	gamma interaction	gamma direct	gamma diffused	readout grains	diffused impact
10μm:	420282	319732	100550	170804	26024
8μm:	420282	319732	100550	98587	8324

Table 1
History of 1000000 single photon events

4.4 Estimation of performance by simulation

To illuminate the possibilities of SSG HDM PET two different grains suspensions and corresponding electronic tuning are considered: the first one with 10μm radius tin grains and with an electronic threshold corresponding to the magnetic flux penetration in one grain, the second with 8μm radius tin grains. We presume working at a temperature (between 200 and 500 mK) allowing a ΔH_{max} of 5 eV. With an electronic threshold corresponding to two simultaneously flipping grains, the performance for each situation is given below for 10^6 events, by the following numbers presented in Table 1:

If we suppress the phantom and the depth of the vessel, we get 384990 gamma's directly in our system. Of these 384990, 367770 are on the 511keV as entry energy. In the system with phantom and vessel, we get 267670 photons with 511 keV. But, in reality, a large fraction of photons give a signal in the same angle as the direct photons. We consider the threshold angle for diffused gammas as 0.234 radians.

The probability of escape P can be evaluated to 0.73.
The probability of direct impact is 0.88.
The solid angle of our system is for 20 cm of length of the detector and 5 cm of radius:

$$4\pi(1-\cos(\arctan(0.5)))$$
$$= 4\pi(1-\frac{2}{\sqrt{5}})$$

and

$$g_r = \frac{2}{\sqrt{5}} = 0.9$$

ϵ is the product of the materialisation factor by the electronic efficiency which is given by Table 2.

The gamma materialization factor is m = 0.367770/0.9=0.419
This gives:
For a radius of 10 μm, ϵ = 0.419*0.534=0.2036
For a radius of 8 μm, ϵ = 0.419*0.380=0.1520

radius	true	diffused	scatter fraction
10 μm	170804/319732 0.534	26024/100550 0.26	26024/170804 0.1523
8 μm	98587/319732 0.380	8324/100550 0.083	8324/98587 0.08443

Table 2
Photon electronic efficiency

This allows us to estimate the

$$NECR = True \frac{1}{1 + f_s + 2\rho \cdot g_t \cdot \tau}$$

with:

$$\tau = 10^{-8}, g_t = 0.9, P = 0.73$$

and:

$$True = \rho \cdot \epsilon^2 \cdot g_t \cdot P^2$$

The maximum acquisition rate is of 10^8, this gives, for a source of 10^8 like the one cited in reference [3]:

For 10 μm radius,

$$\epsilon = 0.2036, True = 1.9810^6$$

$$NECR = \frac{0.019810^8}{1.1523 + \rho 1.8 \cdot 10^{-8}} = 0.66 \cdot 10^6$$

For 8 μm radius,

$$\epsilon = 0.1520, True = 9.10^5$$

$$NECR = \frac{0.00910^8}{1.08443 + \rho 1.8 \cdot 10^{-8}} = 0.3 \cdot 10^6$$

The number of diffused, *Scatter*, is 3. 10^5 and 0.7 10^5 respectively in these two cases.

The number of random coincidences, *Random*, is the most important noise: with such a source of 10^8, and a window of 10 nanosecond, we get 0.9 10^6 an 0.54 10^6 respective of noise.

Improvement of the NECR can be achieved by following paths:

The g_t factor can be increased by a new geometry covering a larger solid angle.

The NECR is proportional to the square of the materialization factor: with three sheets of detecting rows, we should get an electronic efficiency of 0.784 instead of 0.4, this implies a multiplication of the NECR of about 4: this should give:

radius	10^8	10^7	10^6
10 μm	666000 33%	150000 75%	17500 82%
8 μm	300000 30%	71000 80%	8200 90%

Table 3
NECR according to the intensity of the source (10^6, 10^7 and 10^8 Becquerel), and to the radius of the grains, given in counts per second and percentage of the whole counting rate.

NECR= 2.6 10^6 for 10 μm radius, and NECR= 1.2 10^6 for 8 μm radius.
Noise reduction is improved with sharper time coincidences: we take 10^{-8} second.
Increasing electronic efficiency can be achieved in more sophisticated reconstruction taking into account when two cells give a signal.

In usual case, sources of lower intensity are used, in this case we get a more efficient NECR (Table 3, for 1 sheet of row):

5 Elements of comparison with others systems

Existing microPET camera or proposed systems are generally using scintillators, mosaics of small crystal with diodes, big crystals with collimators, and Multi Wire Proportional Chambers.

Some crucial parameters can be pointed out, after a brief evaluation:

- Spatial resolution and high counting rates are of great interest for in vivo dynamic studies. A high density detector minimizes the diffusion by Compton effect relative to photoelectric absorption (reference [4]). Using Litharge gives better accuracy, thanks to the high atomic number of lead. A high density detector system allows simultaneously a great efficiency of gamma materialisation, and the use of a collimator can be avoided (reference [5]). Litharge density is 9.35, to be compared with the densities of detecting materials in advanced cameras (reference [4] and [6]: BGO density is 7.13, LSO density is 4.54, and YAP one is 5.37).
- Here, our calculations were done with a solenoid of 0.2 mm radius and 7 mm length. There are no technical limitations to using narrower solenoids. If we decrease the radius, smaller grains would be read, allowing better energy resolution. Furthermore the coil inductance would be smaller, thus offering shorter dead time.

To a newcomer, cryogenics can be taken as an additional complexity in an advanced system. Let us remember that for liquid Xenon (reference [7]), cryogenics is also mandatory and more generally one can observe that the wide availability of NMR imaging systems makes liquid Helium a common liquid in the medical environment today.

6 Use of SSG cells for gamma-gamma physic in large electron positron colliders

6.1 Physical Problem: gamma-gamma Tagging

In the electron positron future colliders, gamma-gamma tagging is an important challenge. This needs to tag coincidence high energy electrons (between 10 GeV and 500 Gev) at very wmall angle around the beam, in both side of the interaction region. High background coming from halo, beam-gaz interaction and beam-black body interaction has to be support by such a detector which shall cover between 2 an 5 milliradians aperture.

6.1.1 the beam

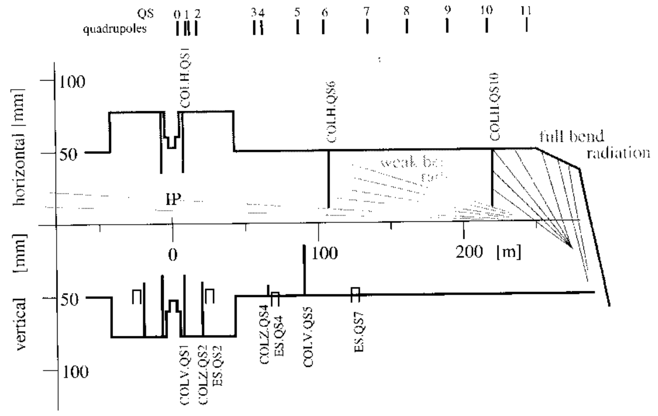

Figure 2: Schematic layout of a straight section at an interaction point (IP) of LEP in the horizontal (top) and vertical (bottom) planes. Shown are the locations of the quadrupoles (QS), electrostatic separators (ES) and collimators (COLH, COLV, COLZ). The solid lines mark the inner vacuum chamber radii.

4

Fig. 15. Collider interaction profile

6.2 Detecting mode

Above a certain energy, the energy loss does not depend of the energy, it is about a constant ([8])

We can choose a smaller depth of the detector, depending which magnetic field, which temperature, we implement, and how many grains we intent to be able to read.

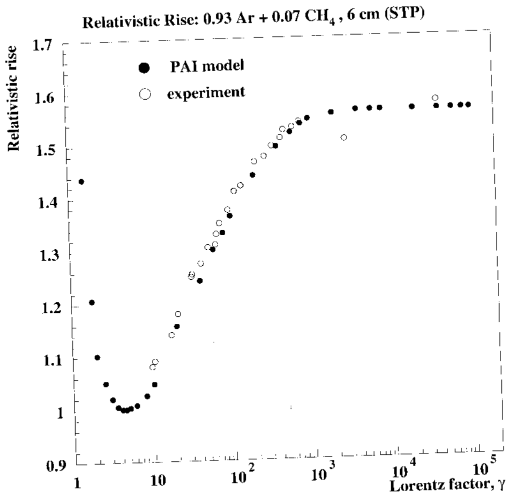

Fig. 16. Relativistic Energy Loss from Grichine

grains	litharge 1Gev	litharge 500 Gev	parafine 1 Gev	parafine 500Gev	parafine 100 Mev	parafine 10 Mev
1	69.4	70.	57.	56.	57.	51.
2	44.	45.95				
3	34	35	30	30		
20	13	13	12.2	12.3	12.2	9.3
40	8.8	8.8	8.7	8.6	8.7	6.4
60	4.8	5.3	4.3	4.5	4.3	3.7
80	3.1	3.1	3.			
100	3.	3.	3.			
global loss	93.2	94.8	17.69	17.6		

Table 4
Energy loss in the grains for dielectric and electron energy

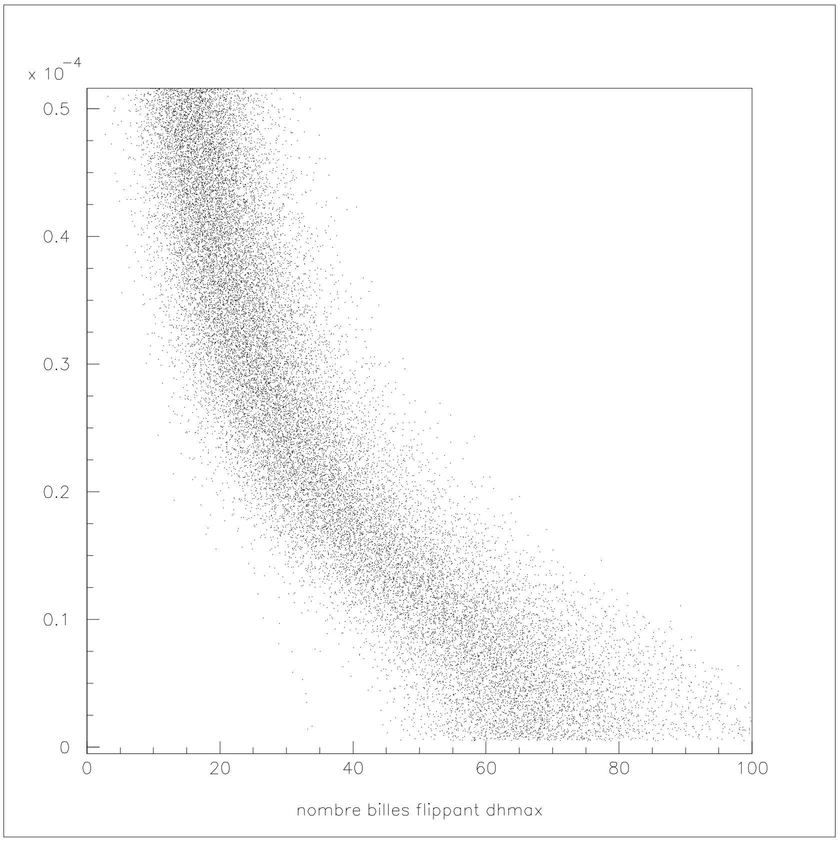

Fig. 17. Grains read in function of dhmax

7 Conclusion

- SSG-HDDM are radiation resistant, efficent, compact, simple and fast detector, it can be used for tagging and geometrical identification.
- Coincidence mode is usefull for various application, high energy and PET
- Developpements are needed to increase capacities, simulates detection operating modes: experiment, simulation (GEANT IV).

References

[1] R. Bruère Dawson et al. Conventional readout electronics for superheated superconducting grains, first experimental results. *Nuclear Instruments and Methods in Physics Research*, pages 211–216, 1989.

[2] H. Dubois. *Rupture de la surchauffe supraconductrice dans des suspensions de microsphères d'étain à très basse temperature.* PhD thesis, Université Paris VI, 1996.

[3] J.S. Huber and W.W. Moses. Conceptual design of a high sensitivity small animal pet camera with 4π coverage. *IEEE Trans. Nuc. Science*, page 498, 1999.

[4] R. H. Huesman S. E. Derenzo, W. W. Moses and T. F. Budinger. Critical instrumentation issues for $<$ 2 mm resolution high sensitivity brain pet. *Quantification of Brain Function*, pages 25–37, 1993.

[5] D. A. Weber and Marijana Ivanovic. Ultra-high-resolution imaging of small animals: implications for preclinival and research studies. *Journal of Nuclear Cardiology*, pages 332–44, 1999. page 334 table of scintillators, page 339, PET performances.

[6] A. Del Guerra and N. Belcari. Advances in animal pet scanners. *The Quartely Journal of Nuclear Medicine*, pages 35–47, 2002.

[7] Jan Sebastien. Developpement tep a xenon liquide. *Seminaire CEA-DAPNIA*, 2002.

[8] V.M.Grichine. Relativistic particle energy loss. *Lecture given at Geant IV user Workshop, SLAC, February 17-22, 2002*, page 183, 2002.